Supporting informantion for

Stable Cellulose-based Porous Binary Metal-Organic Gels as Highly Efficient Adsorbents and Their Application in Adsorption bed for Chlortetracycline Hydrochloride Decontamination

Meijun Liu, [a] Donglei Zou,[a] Taigang Ma,[a] Zhi Liu,[c] Haiyang Yu,[a] Yangxue Li,[*a,b] and Zhen-An Qiao[*d]

[a] *Key Lab of Groundwater Resources and Environment, Ministry of Education, Jilin University, 2519 Jiefang Road, Changchun 130021, P. R. China. Email: yangxueli@jlu.edu.cn*

[b] *State Key Laboratory of Superhard Materials, Jilin University, 2699 Qianjin Street, Changchun 130012, P. R. China*

[c] *School of Municipal and Environmental Engineering, Jilin Jianzhu University, 5088 Xincheng Street, Changchun 130118, P. R. China*

[d] *State Key Laboratory of Inorganic Synthesis and Preparative Chemistry, Jilin University, 2699 Qianjin Street, Changchun 130012, P. R. China*

Contents:

Tables:

Experimental Section

1. Reagents and materials

All reagents and solvents obtained were of analytical grade and used without further purification except 4,4',4''-s-triazine-2,4,6-triyl-tribenzoate (TATB). Dimethyl sulphoxide (DMSO), ferric nitrate nonahydrate ($Fe(NO_3)_3 \cdot 9H_2O$) and aluminium nitrate nonahydrate ($Al(NO_3)_3 \cdot 9H_2O$) were purchased from Sinopharm Chemical Reagent Co., Ltd. (Shanghai, China). The organic reagent TATB was obtained from Alpha Chemical Co., Ltd. (Zhengzhou, China).

2. Characterization

The Brunauer–Emmett–Teller (BET) surface area and porous structure were measured using an ASAP 2020 V3.01 H apparatus (Micrometritics Instrument Corp., USA). The morphologies of the JLUE-MOG aerogels were probed by Field-scanning electron microscopy (SEM, JEOLJXA-840, 15 kV) and transmission electron microscopy (TEM, FEI Tecnai T20). The powder X-ray diffraction (PXRD) spectra of the JLUE-MOG aerogels were performed by a Riguku D/MAX2550 diffractometer using CuKα radiation, 40 kV, 200 mA with scanning rate of 4 ^{o}/min. The X-ray photoelectron spectroscopy (XPS) was conducted using ESCALAB 250Xi X-ray photoelectron spectroscopy. The fourier transform infrared spectra (FT-IR) of the JLUE-MOG aerogels were measured on a Nicolet Nexus 410 infrared spectrometer spectrum instrument using the KBr method ranging from 4000 to 400 cm^{-1}. The thermogravimetric analysis (TGA) was recorded by heating the JLUE-MOG aerogels at a rate of 10 ^{o}C/min in a nitrogen flow. The zeta potential of JLUE-MOGs was measured using a zeta potential meter (Zetasizer nano-ZS90, Malvern) at 25 ^{o}C.

3. Synthesis of JLUE-MOG-3

TATB (0.35 mmol, 0.1576 g) was dissolved into 5 mL DMSO, while $Fe(NO_3)_3 \cdot 9H_2O$ (0.38 mmol, 0.1515 g) and $Al(NO_3)_3 \cdot 9H_2O$ (0.13mmol, 0.0469 g) were co-mixed in 1 mL ethanol. The transparent liquid was mixed together quickly and transferred to a

vacuum drying chamber at 120 ^{o}C for 24 h. Afterwards, a reddish brown transparent gel (JLUE-MOG-3) was formed. Then the resulting wet gel was turned into orange-yellow aerogel powder through freeze-drying procedure. The yield of JLUE-MOG-3 aerogel powder during the synthesis procedure was approximately above 97.5%.

4. Synthesis of JLUE-MOG-4

TATB (0.35 mmol, 0.1576 g) was dissolved into 5 mL DMSO, while $Fe(NO_3)_3{\cdot}9H_2O$ (0.26 mmol, 0.1082 g) and $Al(NO_3)_3{\cdot}9H_2O$ (0.26mmol, 0.1005 g) were co-mixed in 1 mL ethanol. The transparent liquid was mixed together quickly and transferred to a vacuum drying chamber at 120 ^{o}C for 24 h. Afterwards, a yellow brown transparent gel (JLUE-MOG-4) was formed. Then the resulting wet gel was turned into yellow aerogel powder through freeze-drying procedure. The yield of JLUE-MOG-4 aerogel powder during the synthesis procedure was approximately above 97.5%.

5. Synthesis of JLUE-MOG-5

TATB (0.35 mmol, 0.1576 g) was dissolved into 5 mL DMSO, while $Fe(NO_3)_3{\cdot}9H_2O$ (0.13 mmol, 0.0505 g) and $Al(NO_3)_3{\cdot}9H_2O$ (0.38mmol, 0.1407 g) were co-mixed in 1 mL ethanol. The transparent liquid was mixed together quickly and transferred to a vacuum drying chamber at 120 ^{o}C for 24 h. Afterwards, a light-yellow transparent gel (JLUE-MOG-5) was formed. Then the resulting wet gel was turned into light yellow aerogel powder through freeze-drying procedure. The yield of JLUE-MOG-5 aerogel powder during the synthesis procedure was approximately above 97.5%.

6. Synthesis of cellulose aerogels

5 g microcrystalline cellulose was mixed with 40 g water and kept for 0.5 h at 5 ^{o}C. In the meantime, 7.6 g NaOH was dissolved in 47.4 g water and precooled at -4 ^{o}C before added into cellulose/water solution. Vigorous mixing procedure was conducted in -4 ^{o}C for 0.5 h. Then, the transparent solutions were poured into cylindrical moulds and placed at 50 ^{o}C for 2 h until totally gelation (cellulose/NaOH/water gels). Afterwards, regeneration procedure was established when cellulose/NaOH/water gels were

immersed into 50 °C water, and ended until the colour of gels turned from yellow to white. After freeze drying, cylindrical cellulose aerogels were obtained for further experimentation.

7. Synthesis of JLUE-MOG-4@cellulose aerogels

The procedures were the same as the synthesis of JLUE-MOG-4, except the addition of the freeze-dried cylindrical cellulose aerogels (white) taken from 96-well plate. After freeze drying, the cylindrical yellow JLUE-MOG-4@cellulose aerogels were obtained for the following research.

8. Adsorption experiments

To evaluate the adsorption capacity of the JLUE-MOG aerogel powders, the following tests were performed. For the adsorption kinetics, 30 mg of dried JLUE-MOG aerogel powders were added into the reactors containing 30 mL of 100 $mg \cdot L^{-1}$ CTC solution of pH=6 and placed in an incubator at 25 °C without light exposure. In addition, the impacts of various adsorbent dosage and different initial pH on CTC adsorption removal were investigated. Besides, for the adsorption isotherms, 30 mg JLUE-MOG aerogels were separately put into 30 mL CTC solution with increasing concentration at pH=6, and placed in 15 °C, 25 °C and 35 °C for evaluating the maximum adsorption capacities under the corresponding temperature condition. At certain intervals, the samples were collected from each reactor and filtrated by using 0.22 μm syringe membrane filters. The residual concentration of CTC was measured under the maximum adsorption wavelength of 364 nm. The amount CTC adsorbed at equilibrium was calculated by equation as below:

$$q_e = (C_0 - C_e)\frac{V}{m} \quad (1)$$

$$q_t = (C_0 - C_t)\frac{V}{m} \quad (2)$$

where C_0 is the initial CTC concentration ($mg \cdot L^{-1}$); C_e is the equilibrium concentration of CTC in solution ($mg \cdot L^{-1}$); C_t is the concentration of CTC in solution at time t ($mg \cdot L^{-1}$); V is the total volume of solution used (L) and m is the mass of adsorbent used (g).

9. Experimental design

A four-factor three-level, central composite design (CCD) was carried out by response surface methodology (RSM) with 30 total experimental runs, which consisted of 6 at central points, 8 at axial and 16 at factorial points. The pertinent operating parameters and relevant ranges were decided on the basis of the adsorption performance, while the temperature (A), adsorbent dosage (B), initial pH (C) and initial CTC concentration (D) were chosen in this research. The experiments were performed randomly in order to avoid systematic errors.

Analysis of variance (ANOVA) was applied for determining the various model coefficients and figuring out the significance of model we selected. In this paper, Design-Expert version 8.06 (State Ease, Inc) was used to design experiments and analyse correlation coefficient (R^2), F value, P-value, values of "Prob > F" and “Adeq Precision” through experimental data.

10. The adsorption performance of syringe adsorption units

Syringe adsorption units were established for testing the cellulose aerogels and adsorption capacities of JLUE-MOG-4@cellulose aerogels in small-scale. 10 $mg \cdot L^{-1}$ CTC was regarded as the polluted wastewater during 4 h operation, flowing by its gravity. For the two syringe adsorption units, 0.3 cm quartz sand was packed tightly for supporting layer. 0.48 g cellulose aerogels (2.7 cm in height) and 0.42 g JLUE-MOG-4@cellulose aerogels (2.7 cm in height) were main responsible for the subsequent CTC adsorption. The CTC removal performance (C_t/C_0) and corresponding UV-Vis spectra were investigated for evaluation.

11. The adsorption performance of custom-made adsorption beds

For further evaluating the adsorption ability of JLUE-MOG-4@cellulose aerogels in pilot-scale device, custom-made adsorption bed was conducted by flowing 10 $mg \cdot L^{-1}$ CTC solution through adsorbents by its gravity for 24 h. In this study, quartz sand was utilized for preventing from the erosion and supporting the whole filter materials

layer, which was responsible for 9 cm of height in adsorption bed. In the meanwhile, the weight of effective adsorbents was 1.15 g (15 cm in height) above the supporting layer. More importantly, in order to totally verify the adsorption capacity of JLUE-MOG-4@cellulose aerogels, the blank adsorption bed was established to examine the CTC removal under the same circumstances, except the cellulose aerogels replaced the JLUE-MOG-4@cellulose for CTC capture. During the whole day and night operation, the effluent CTC concentration and CTC removal efficiency after certain running period were investigated. The CTC removal efficiency was calculated for comparison by equation as below:

$$\text{CTC Removal Efficiency}\ (\%) = \frac{C_{\text{influent}} - C_{\text{effluent}}}{C_{\text{influent}}} \times 100\% \quad (3)$$

where $C_{influent}$ is the influent CTC concentration ($mg \cdot L^{-1}$); $C_{effluent}$ is the effluent CTC concentration of custom-made adsorption bed ($mg \cdot L^{-1}$).

Figures

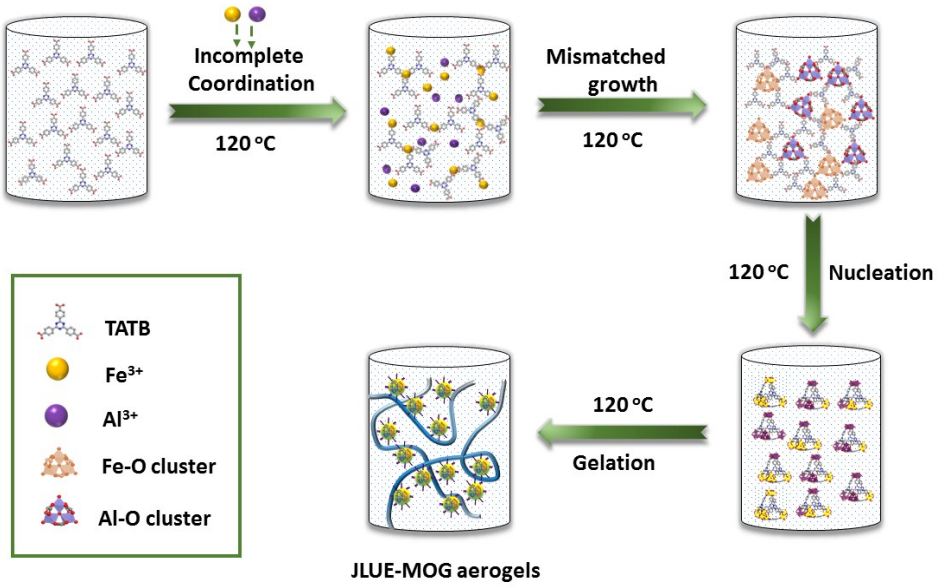

Fig. S1 Schematic representation of the formation of JLUE-MOG aerogels.

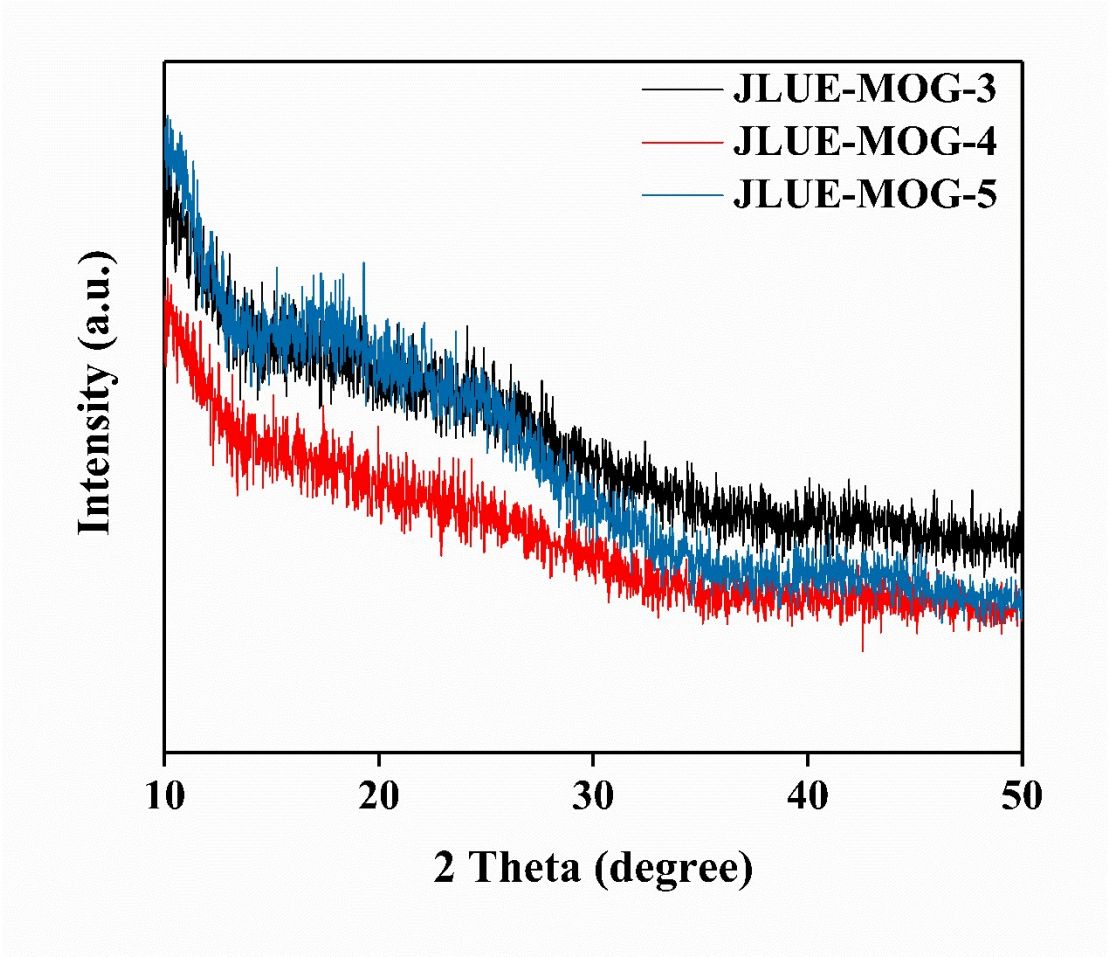

Fig. S2 The XRD patterns of JLUE-MOG-3, JLUE-MOG-4 and JLUE-MOG-5.

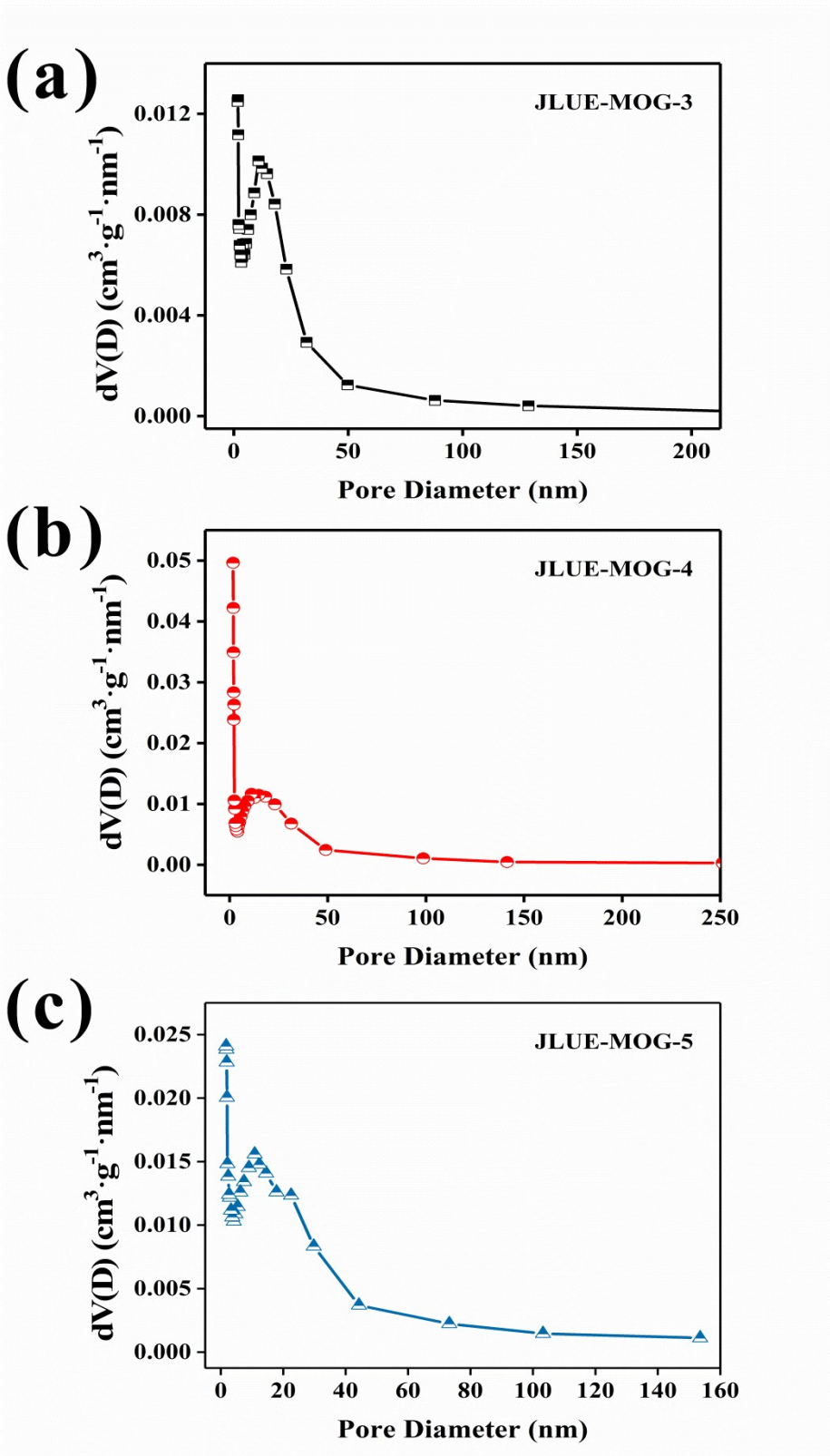

Fig. S3 (a) The pore size distribution of JLUE-MOG-3. (b) The pore size distribution of JLUE-MOG-4. (c) The pore size distribution of JLUE-MOG-5.

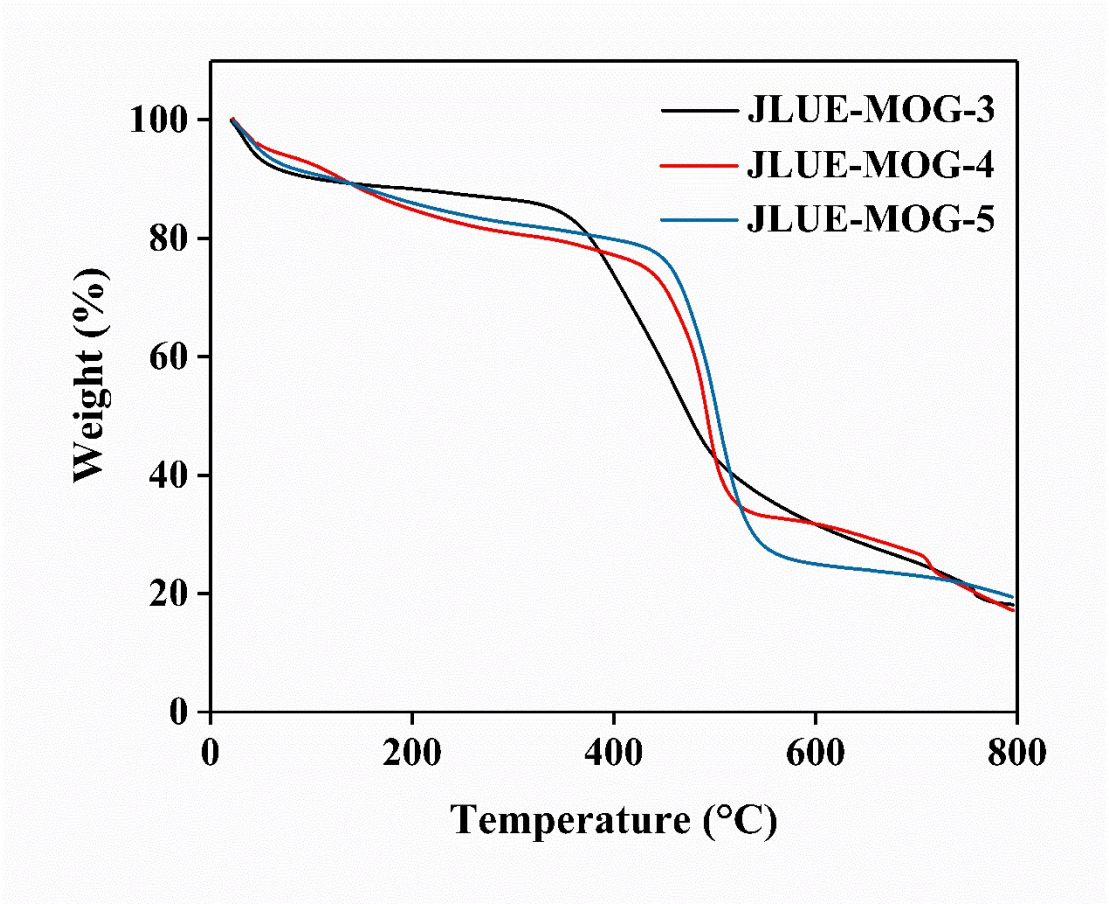

Fig. S4 The TGA curves of JLUE-MOG aerogels.

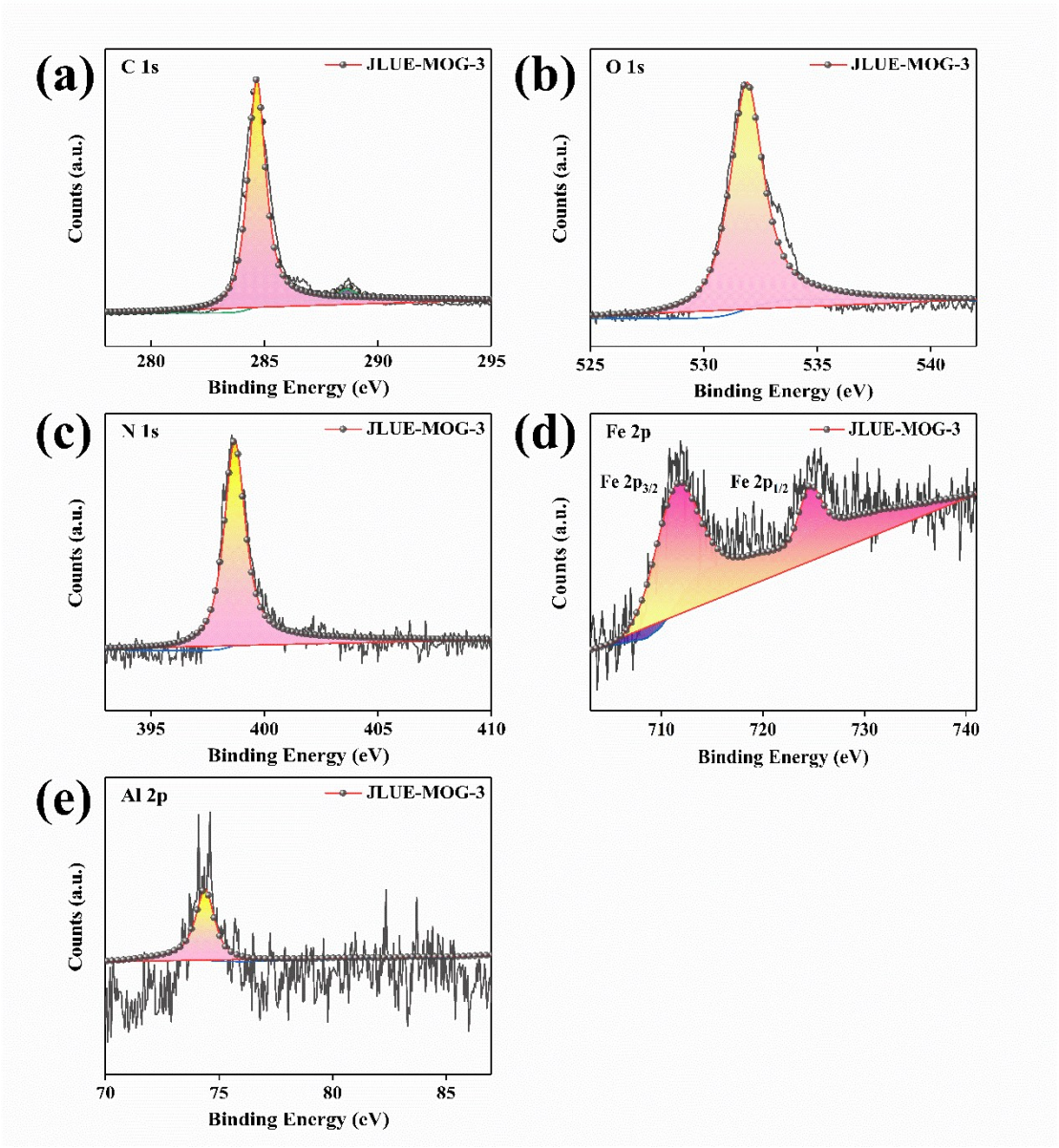

Fig. S5 The XPS spectra of JLUE-MOG-3: (a) High-solution spectrum of C 1s; (b) High-solution spectrum of O 1s; (c) High-solution spectrum of N 1s; (d) High-solution spectrum of Fe 2p; (d) High-solution spectrum of Al 2p.

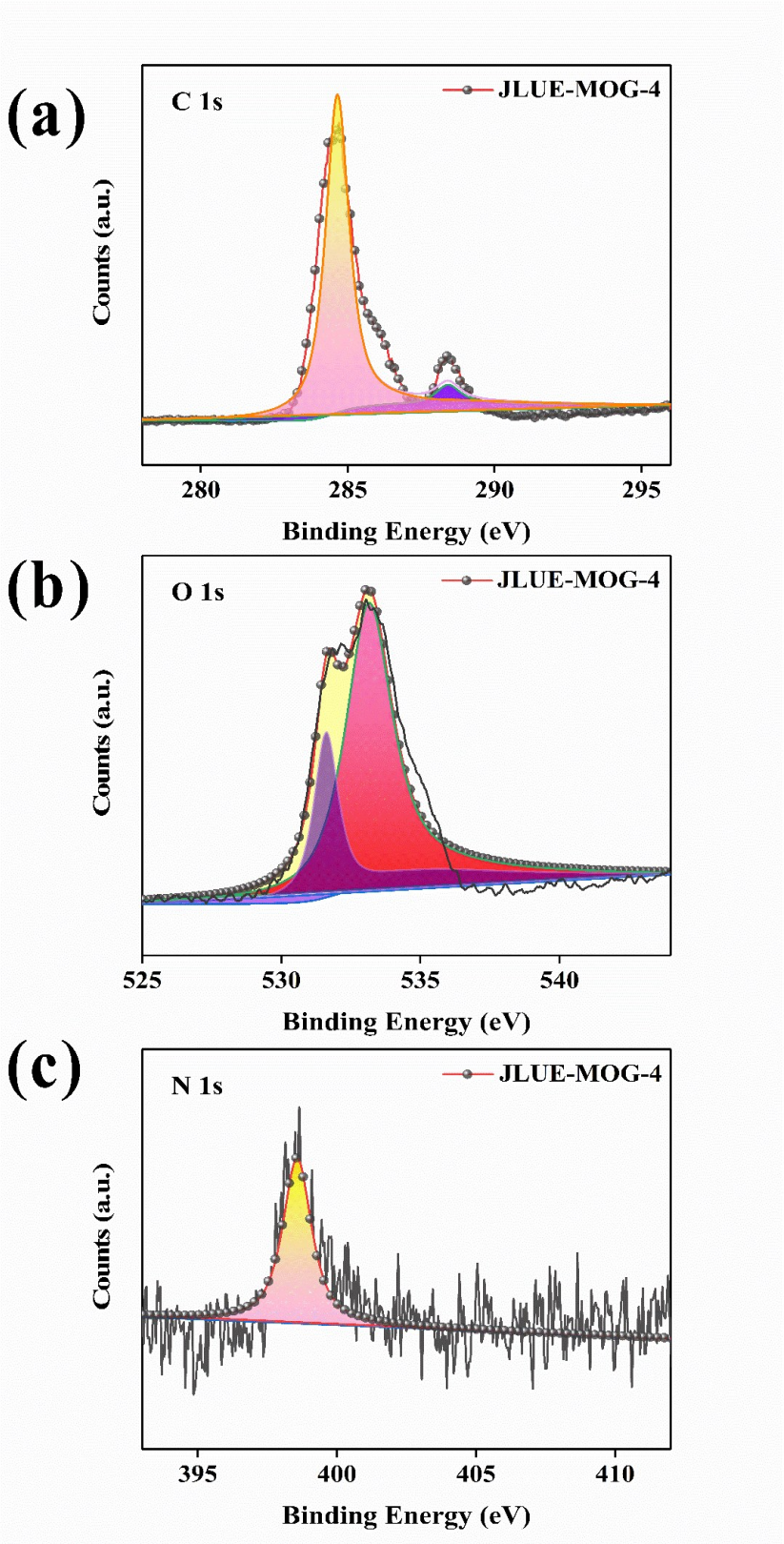

Fig. S6 The XPS spectra of JLUE-MOG-4: (a) High-solution spectrum of C 1s; (b) High-solution spectrum of O 1s; (c) High-solution spectrum of N 1s.

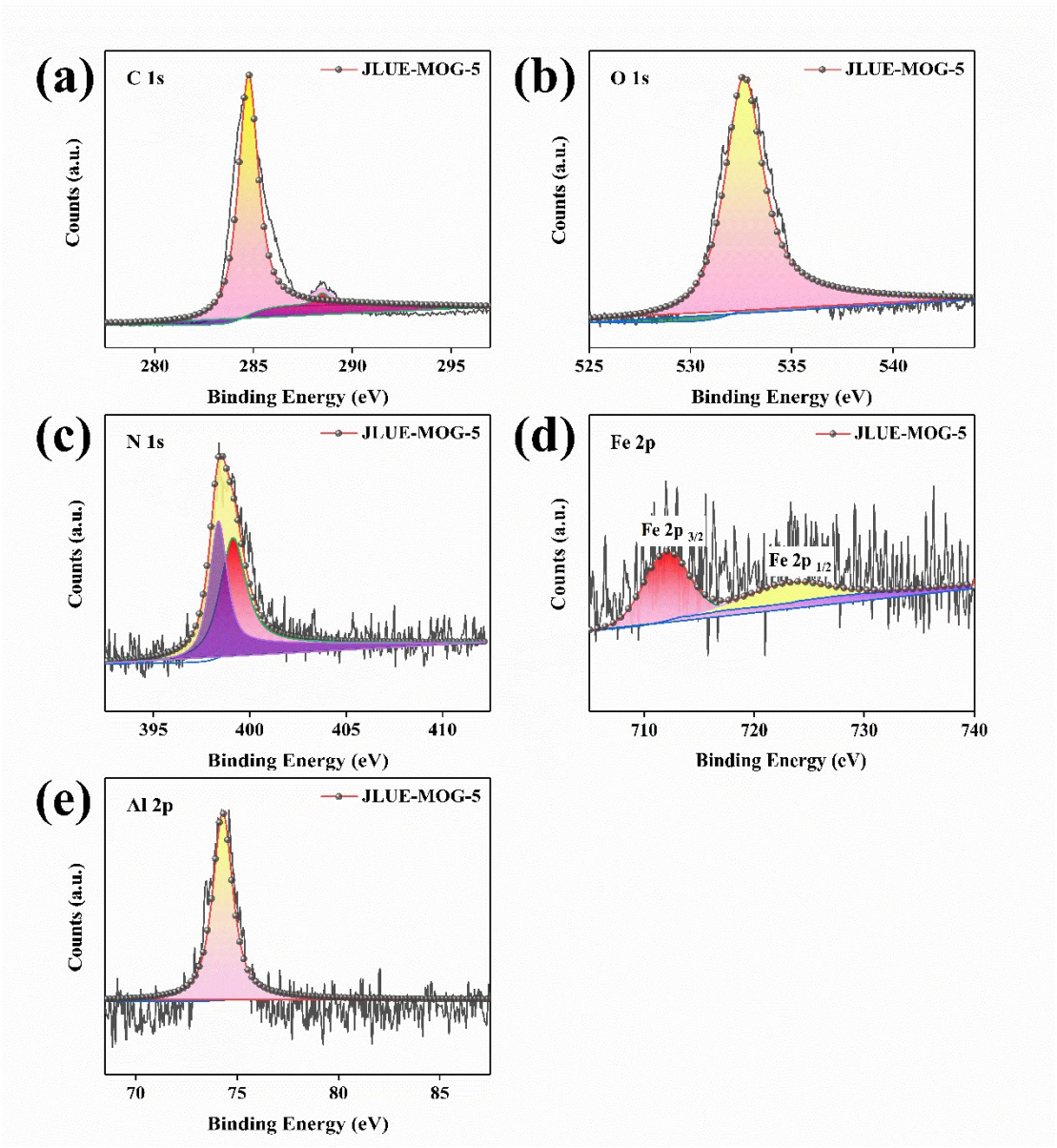

Fig. S7 The XPS spectra of JLUE-MOG-5: (a) High-solution spectrum of C 1s; (b) High-solution spectrum of O 1s; (c) High-solution spectrum of N 1s; (d) High-solution spectrum of Fe 2p; (e) High-solution spectrum of Al 2p.

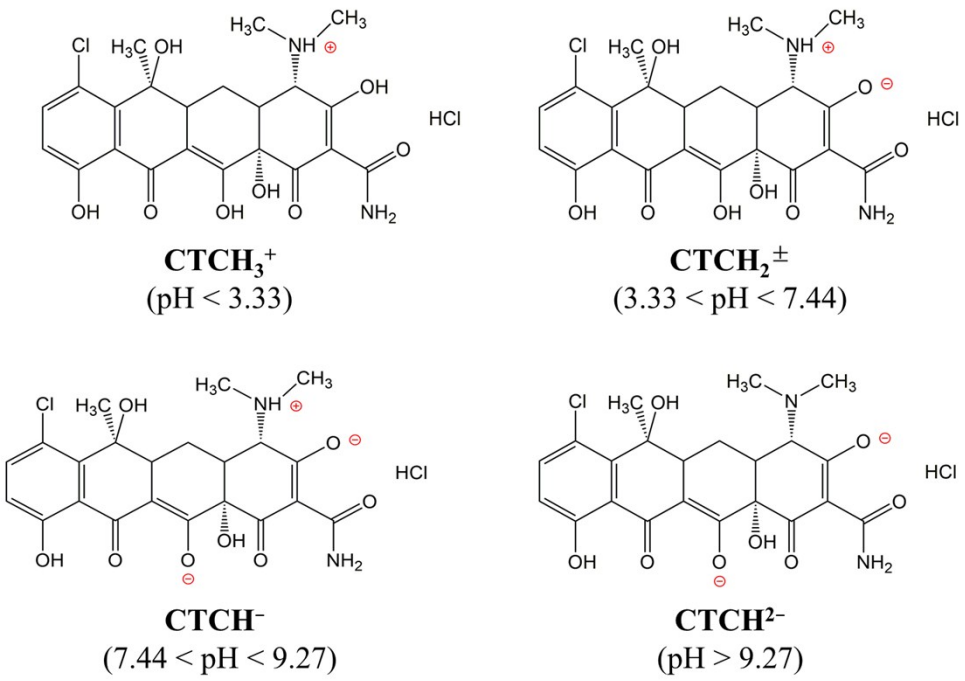

Fig. S8 Different forms of CTC depending on the solution pH.

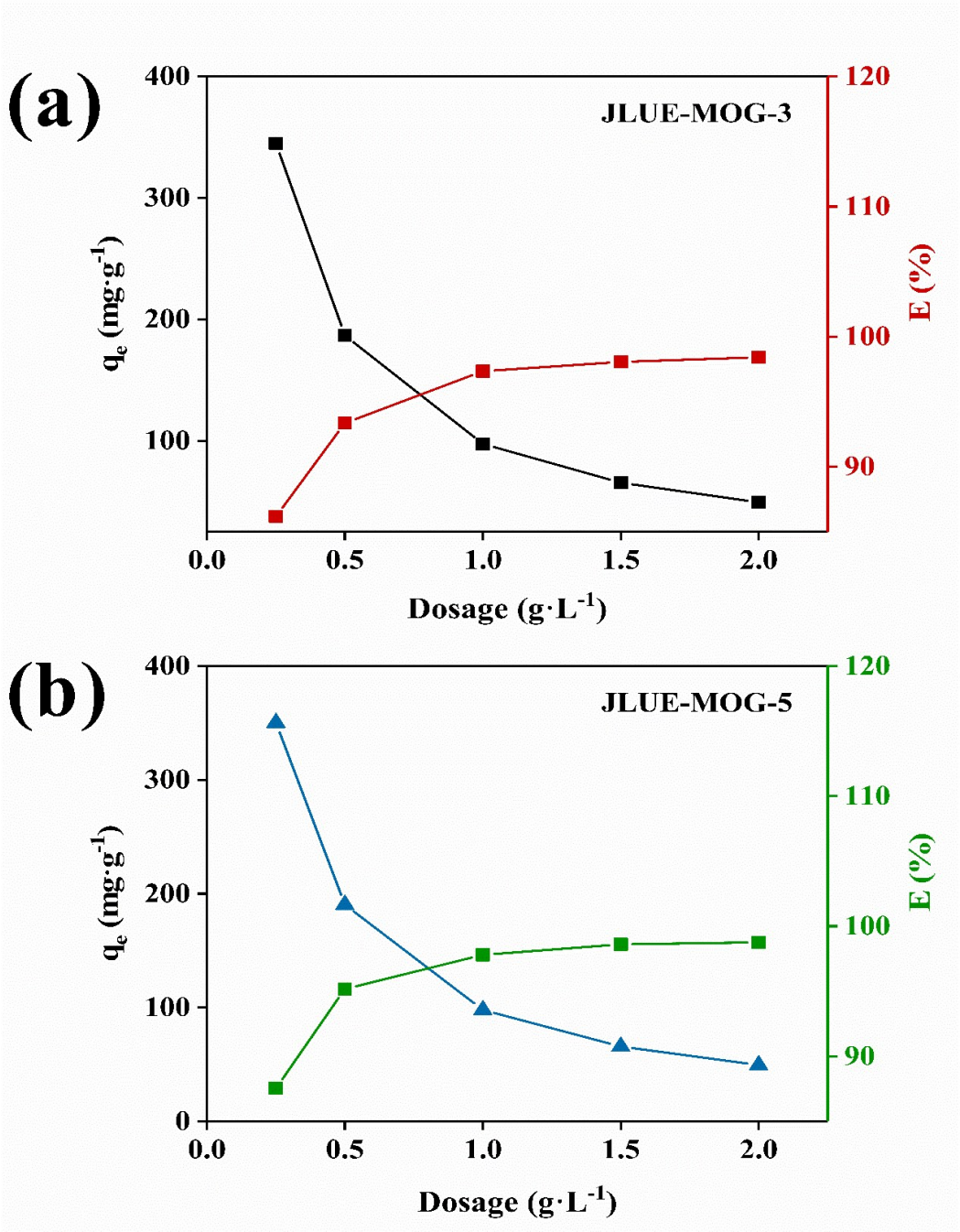

Fig. S9 Variance in the removal efficiency (E) and adsorptive capacity (q_e) of (a) JLUE-MOG-3 and (b) JLUE-MOG-5 as a function of adsorbent dosage.

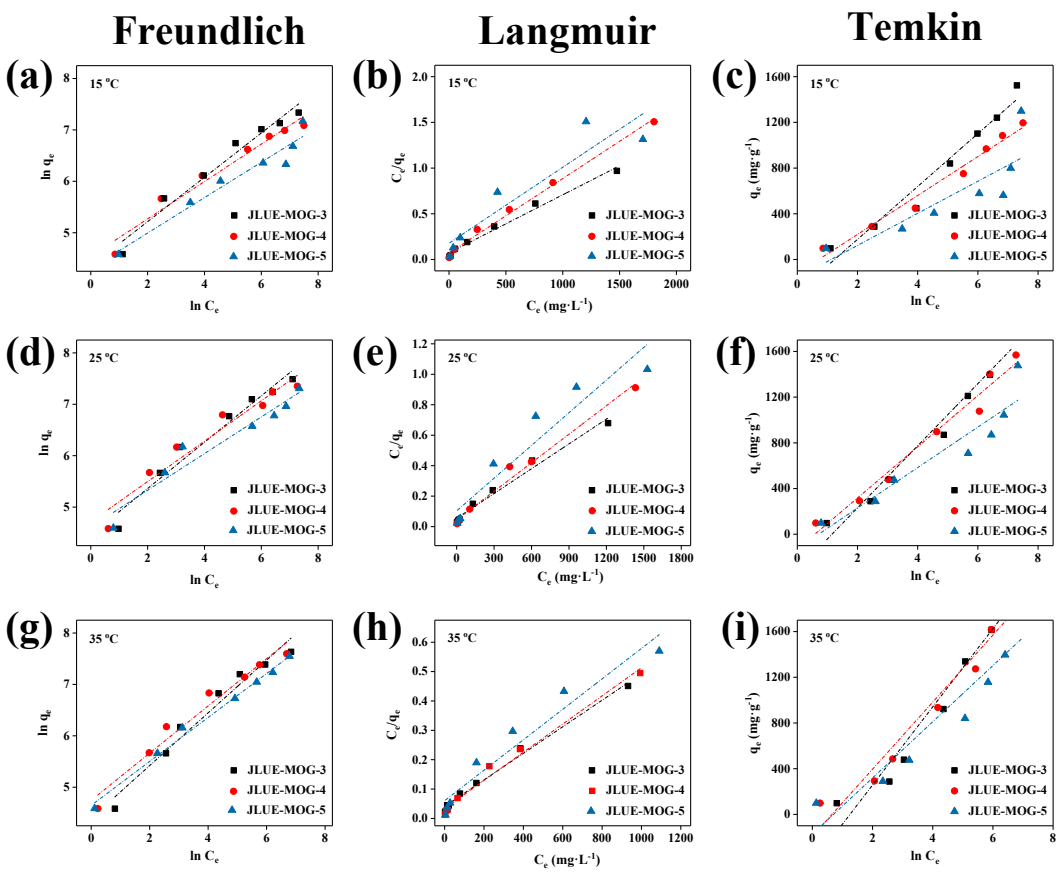

Fig. S10 The Freundlich, Langmuir and Temkin linear fittings for CTC adsorption removal by JLUE-MOG aerogels at three different temperatures, respectively.

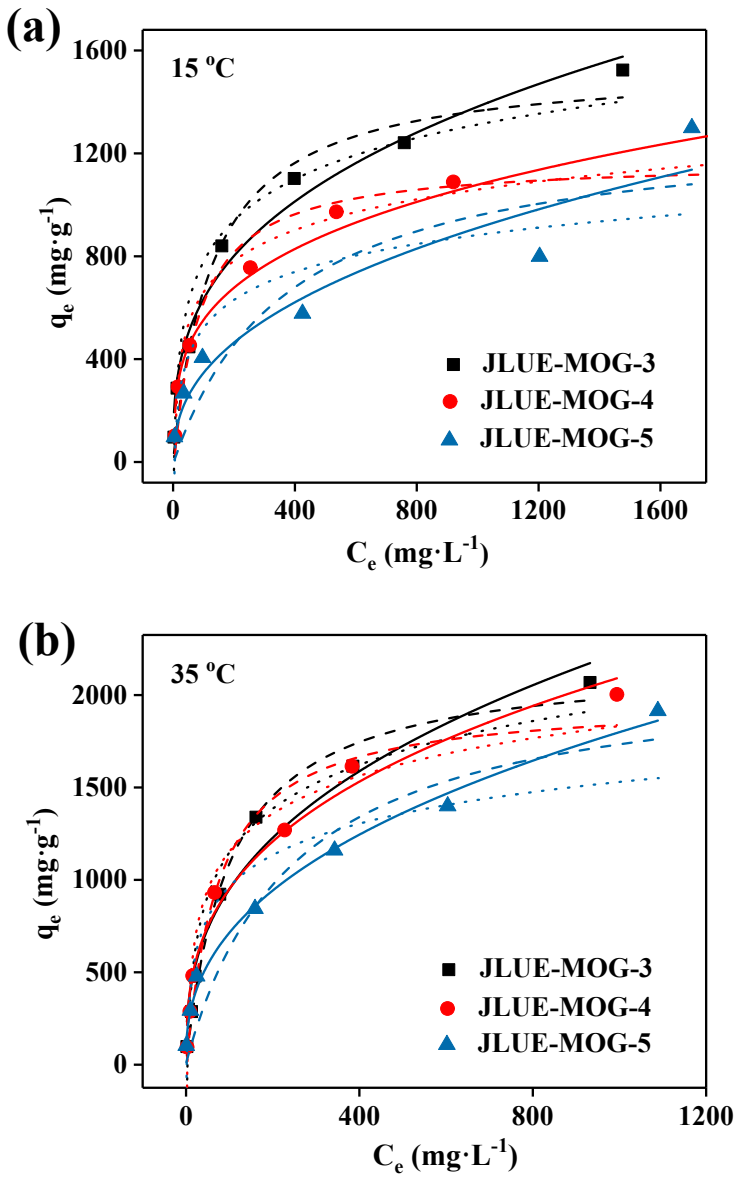

Fig. S11 Data fittings with Langmuir, Freundlich and Temkin adsorption isotherms of CTC adsorption by JLUE-MOG aerogels at (a) 15 °C and (b) 35 °C, respectively. Solid lines represent Freundlich isotherms; dash lines represent Langmuir isotherms; dot lines represent Temkin isotherms.

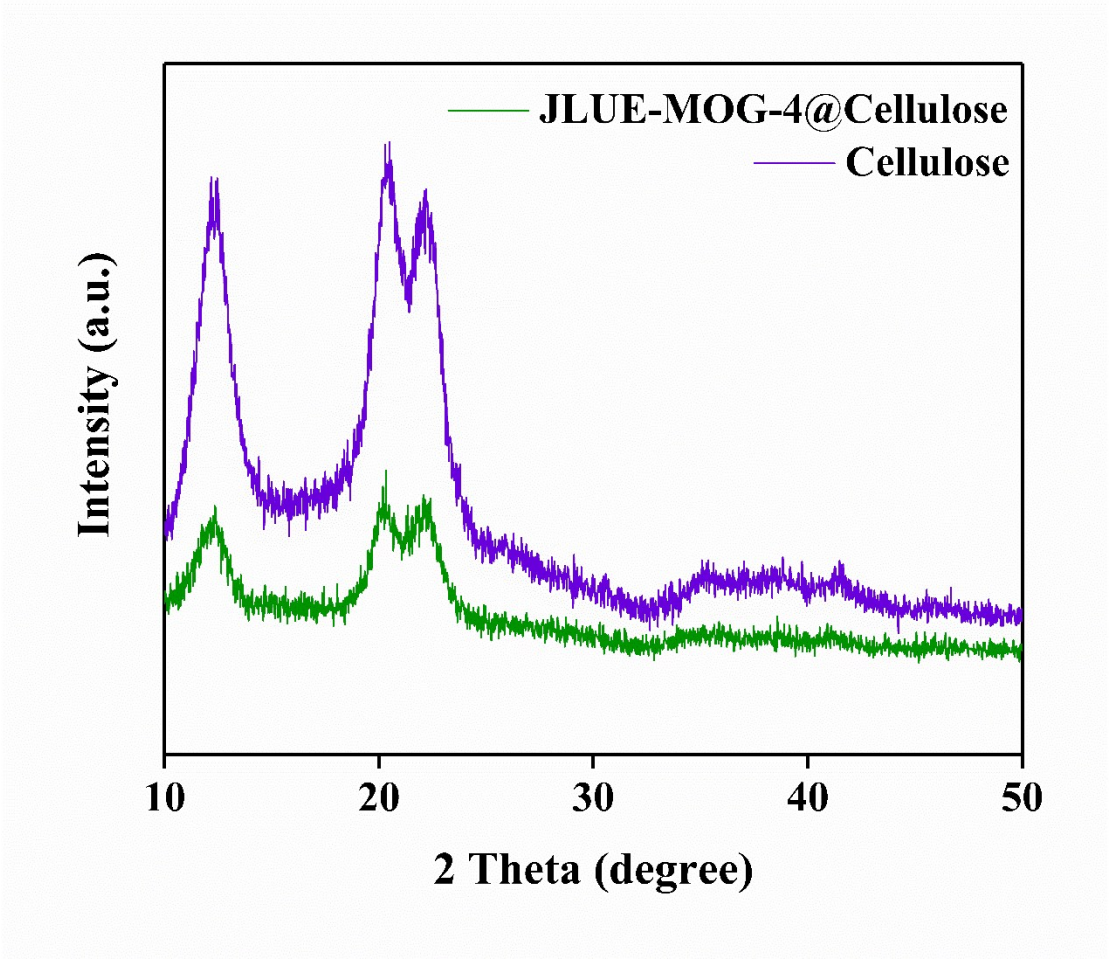

Fig. S12 The XRD patterns of cellulose aerogels and JLUE-MOG-4@cellulose aerogels.

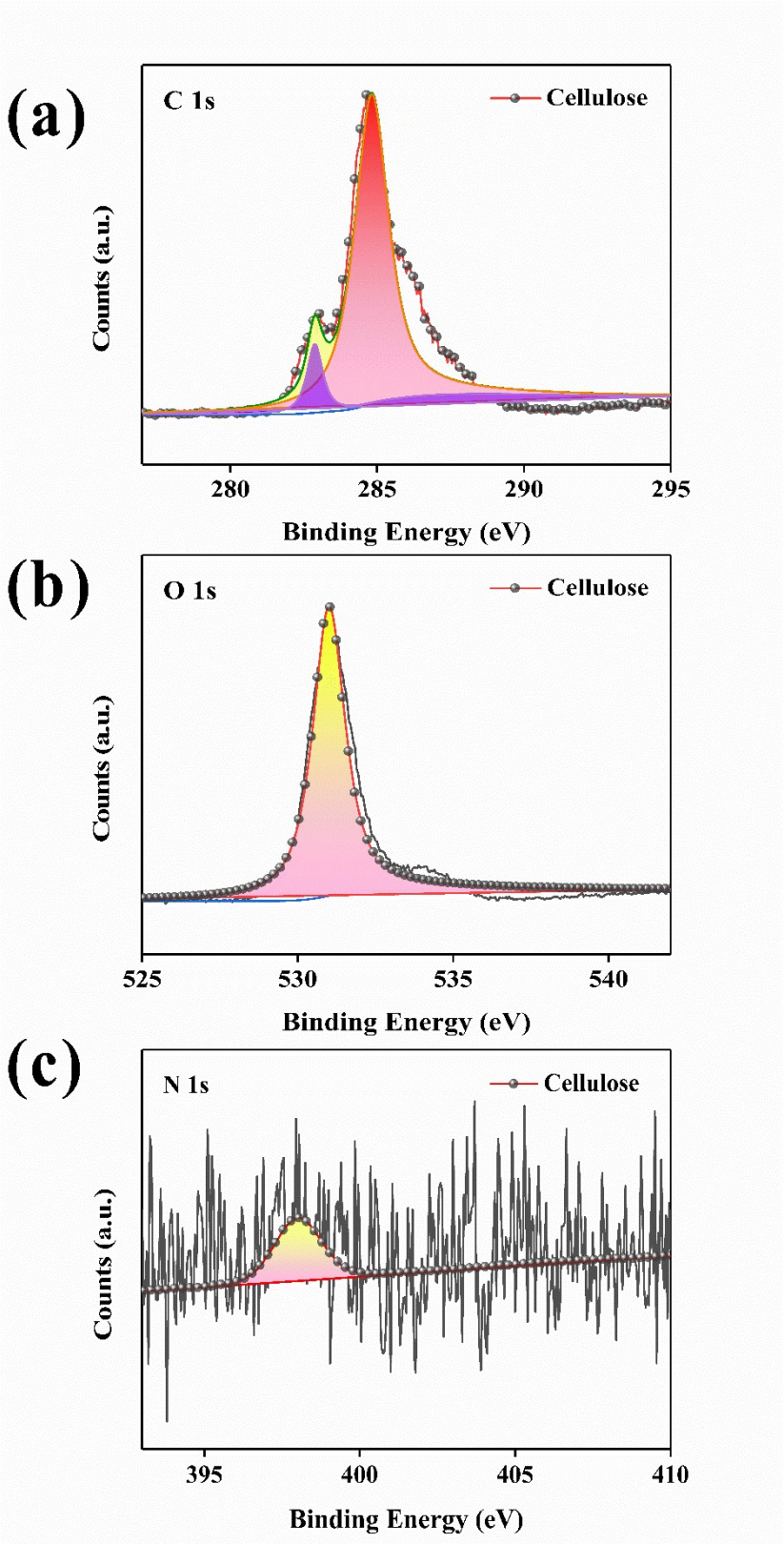

Fig. S13 The XPS spectra of cellulose aerogels: (a) High-solution spectrum of C 1s; (b) High-solution spectrum of O 1s; (c) High-solution spectrum of N 1s.

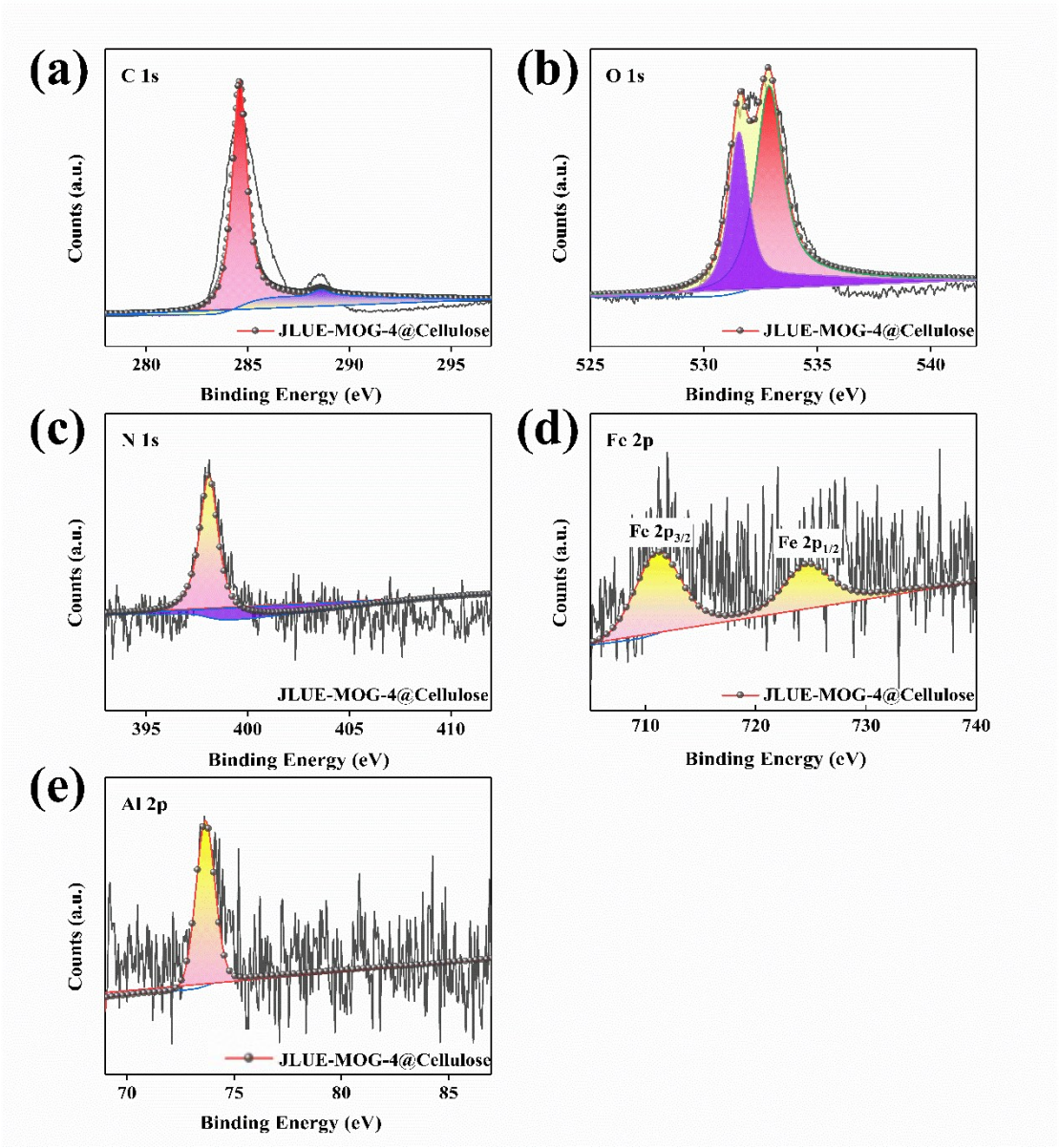

Fig. S14 The XPS spectra of JLUE-MOG-4@cellulose aerogels: (a) High-solution spectrum of C 1s; (b) High-solution spectrum of O 1s; (c) High-solution spectrum of N 1s; (d) High-solution spectrum of Fe 2p; (e) High-solution spectrum of Al 2p.

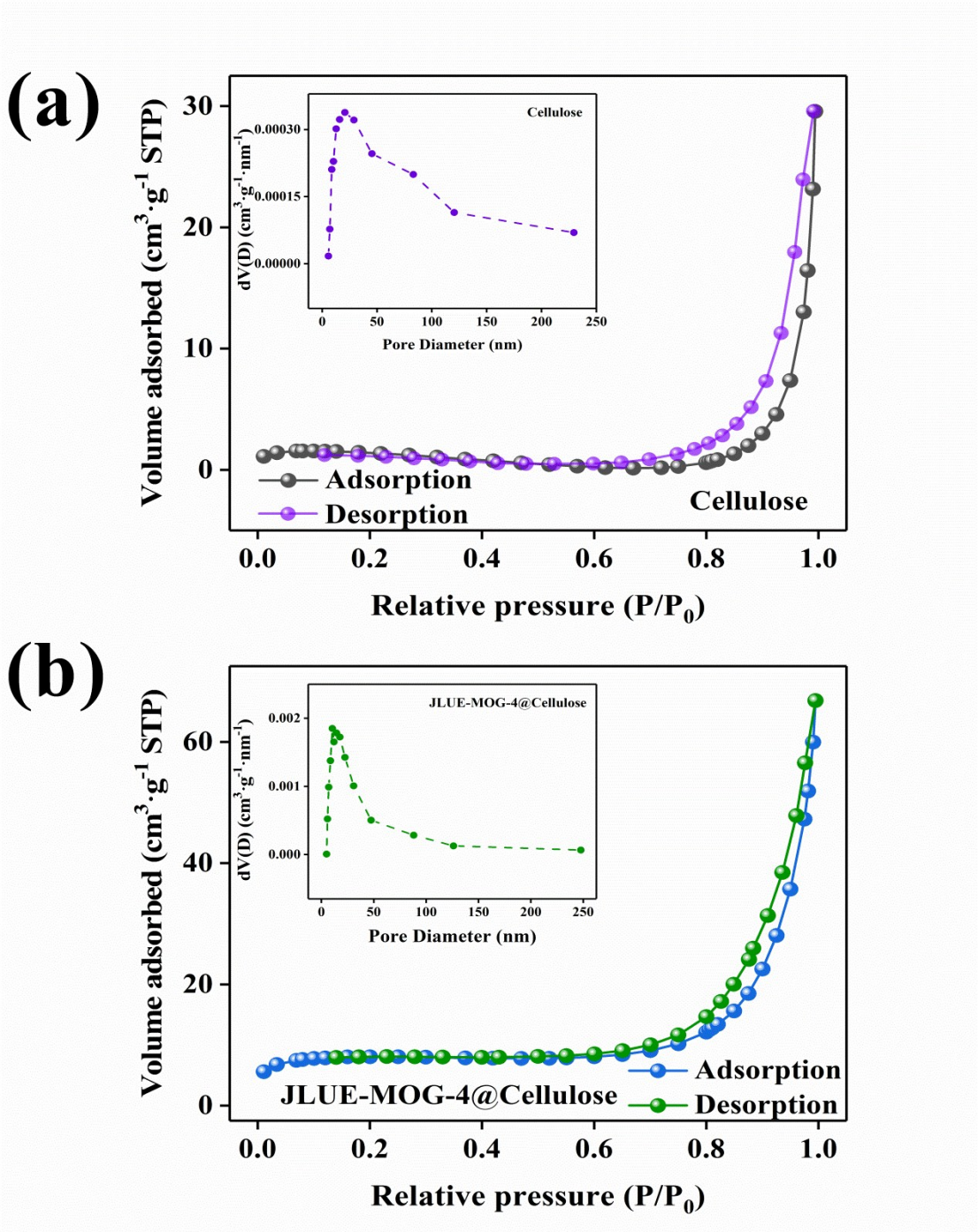

Fig. S15 (a) The BET results of cellulose aerogels. Inserted: The pore size distribution of cellulose aerogels. (b) The BET results of JLUE-MOG-4@cellulose aerogels. Inserted: The pore size distribution of JLUE-MOG-4@cellulose aerogels.

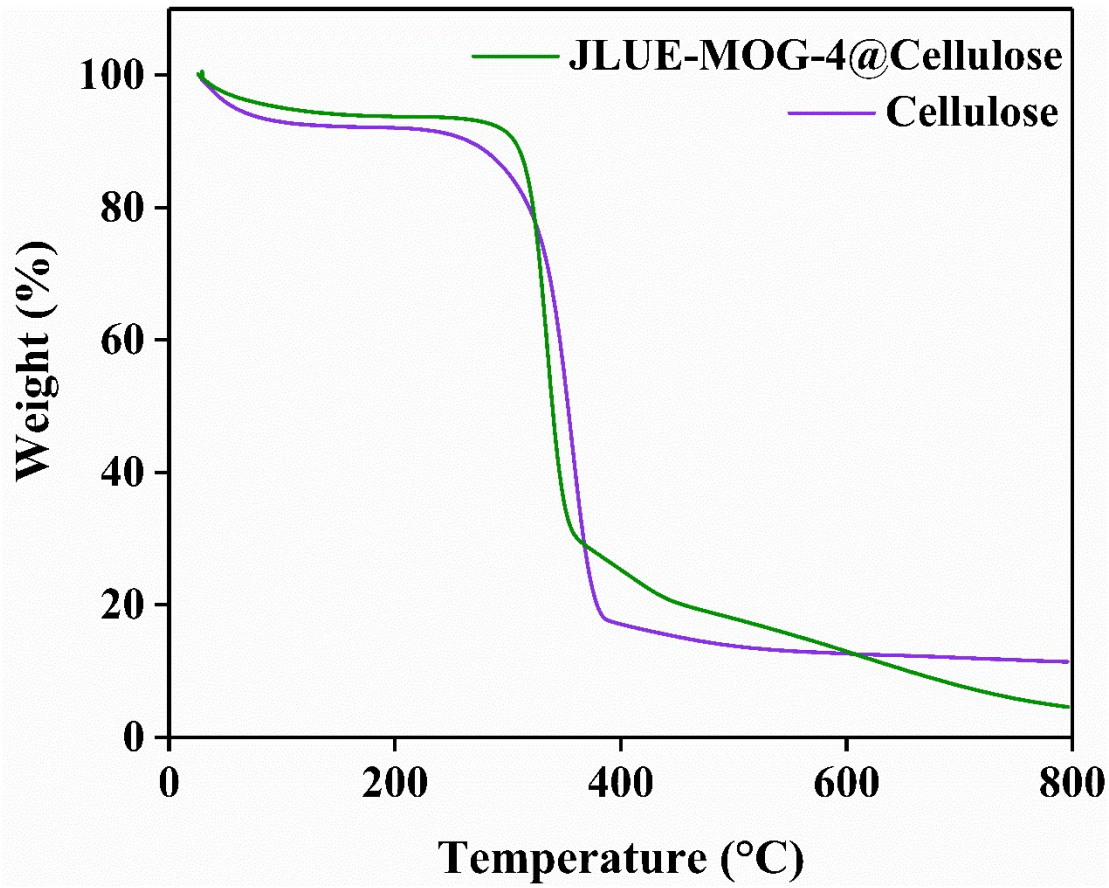

Fig. S16 The TGA curves of cellulose and JLUE-MOG-4@cellulose aerogels.

Tables

Table S1 Pseudo-first-order kinetic model parameters for CTC adsorption by JLUE-MOG-3, JLUE-MOG-4 and JLUE-MOG-5.

JLUE-MOGs	C_0 ($mg \cdot L^{-1}$)	$q_{e,exp}$ ($mg \cdot g^{-1}$)	Removal Efficiency（%）	Pseudo-first-order kinetics			
				k_1 (h^{-1})	$q_{e1,theor}$ ($mg \cdot g^{-1}$)	Δq_1 （%）	R^2
JLUE-MOG-3	50	48.26	96.52	0.92×10^{-1}	20.35	137.15	0.95
	100	97.45	97.45	0.70×10^{-1}	60.58	60.86	0.98
	200	195.23	97.62	0.63×10^{-1}	145.04	34.60	0.99
JLUE-MOG-4	50	48.26	96.52	0.69×10^{-1}	15.86	204.29	0.78
	100	98.06	98.06	0.77×10^{-1}	49.45	98.30	0.97
	200	196.24	98.12	0.62×10^{-1}	129.15	51.95	0.98
JLUE-MOG-5	50	48.06	96.12	0.62×10^{-1}	35.09	36.96	0.99
	100	97.66	97.66	0.61×10^{-1}	74.59	30.93	0.99
	200	196.24	98.12	0.33×10^{-1}	152.36	28.80	0.99

Table S2 Pseudo-second-order kinetic model parameters for CTC adsorption by JLUE-MOG-3, JLUE-MOG-4 and JLUE-MOG-5.

JLUE-MOGs	C_0 ($mg \cdot L^{-1}$)	$q_{e,exp}$ ($mg \cdot g^{-1}$)	Removal Efficiency (%)	Pseudo-second-order kinetics			
				k_2 ($g \cdot mg^{-1} \cdot h^{-1}$)	$q_{e2,theor}$ ($mg \cdot g^{-1}$)	Δq_2 (%)	R^2
JLUE-MOG-3	50	48.26	96.52	0.25×10^{-1}	48.31	0.10	0.99
	100	97.45	97.45	0.49×10^{-2}	97.66	0.22	0.99
	200	195.23	97.62	0.16×10^{-2}	195.96	0.37	0.99
JLUE-MOG-4	50	48.26	96.52	0.25×10^{-1}	48.31	0.10	0.99
	100	98.06	98.06	0.69×10^{-2}	98.16	0.10	0.99
	200	196.24	98.12	0.19×10^{-2}	196.86	0.31	0.99
JLUE-MOG-5	50	48.06	96.12	0.61×10^{-2}	48.21	0.31	0.99
	100	97.66	97.66	0.28×10^{-2}	97.95	0.30	0.99
	200	196.24	98.12	0.72×10^{-3}	194.25	1.02	0.99

Table S3 Intraparticle diffusion model parameters for CTC adsorption by JLUE-MOG-3, JLUE-MOG-4 and JLUE-MOG-5.

JLUE-MOGs	C_0 ($mg \cdot L^{-1}$)	Intraparticle diffusion model					
		$k_{i,1}$ ($mg \cdot g^{-1} \cdot h^{-1/2}$)	C_1 ($mg \cdot g^{-1}$)	R^2	$k_{i,2}$ ($mg \cdot g^{-1} \cdot h^{-1/2}$)	C_2 ($mg \cdot g^{-1}$)	R^2
JLUE-MOG-3	50	6.45	20.32	0.54	0.090	47.20	0.31
	100	14.21	24.27	0.81	0.60	90.34	0.41
	200	29.26	30.58	0.92	1.96	172.10	0.52
JLUE-MOG-4	50	5.42	24.11	0.35	0.11	46.98	0.16
	100	11.90	38.16	0.53	0.41	93.20	0.31
	200	25.73	49.48	0.77	1.77	175.29	0.49
JLUE-MOG-5	50	6.35	9.40	0.85	0.44	42.88	0.45
	100	13.42	15.82	0.90	0.98	85.96	0.54
	200	23.43	22.01	0.93	5.82	123.53	0.79

Table S4 Freundlich, Langmuir and Temkin adsorption isotherm model parameters for CTC adsorption by JLUE-MOG-3, JLUE-MOG-4 and JLUE-MOG-5.

JLUE-MOGs	Temperature (°C)	Freundlich isotherm			Langmuir isotherm			Temkin isotherm		
		n	K_F	R^2	Q_m (mg·g^{-1})	K_L	R^2	A	B	R^2
JLUE-MOG-3	15	2.33	77.48	0.96	1574.8	13.70	0.98	0.29	231.42	0.96
	25	2.22	86.49	0.95	1841.6	18.18	0.98	0.32	271.98	0.97
	35	1.96	81.45	0.96	2212.4	24.39	0.99	0.29	342.28	0.95
JLUE-MOG-4	15	2.78	93.69	0.95	1227.0	13.89	0.99	0.49	170.42	0.98
	25	2.56	112.17	0.93	1600.0	21.74	0.98	0.56	224.08	0.97
	35	2.22	114.43	0.96	2083.3	29.41	0.98	0.52	293.72	0.96
JLUE-MOG-5	15	2.94	74.44	0.93	1203.4	5.56	0.84	0.29	155.83	0.79
	25	2.78	100.48	0.93	1396.7	9.09	0.90	0.49	177.23	0.88
	35	2.38	104.58	0.99	1930.5	16.13	0.93	0.49	246.08	0.89

Table S5 Comparison of CTC adsorption capacity (q_m) by various adsorbents.

Target pollutant	Adsorbents	adsorption conditions	q_m ($mg \cdot g^{-1}$)	References
CTC	Magnetic graphene oxide	pH=4.00-5.00; T=40 °C; adsorbent: 0.07 $g \cdot L^{-1}$;	162.42	1
CTC	GO-Magnetic particles	pH=7.00; T=25 °C; adsorbent: 2.00 $g \cdot L^{-1}$;	42.60	2
CTC	GO/TiO_2	pH=4.00; T=25 °C; adsorbent: 0.20 $g \cdot L^{-1}$;	261.10	3
CTC	GO-CNF	pH= –; T=25 °C; adsorbent: 0.20 $g \cdot L^{-1}$;	396.49	4
CTC	MWCNT/MIL-53(Fe)	pH=7.00; T=25 °C; adsorbent: 0.20 $g \cdot L^{-1}$;	180.68	5
CTC	MIL-53(Fe)	pH=7.00; T=25 °C; adsorbent: 0.20 $g \cdot L^{-1}$;	160.43	5
CTC	NH_2-MIL-53(Fe)	pH=7.00; T=25 °C; adsorbent: 0.20 $g \cdot L^{-1}$;	152.29	6
CTC	MWCNT/NH_2-MIL-53(Fe)	pH=7.00; T=25 °C; adsorbent: 0.20 $g \cdot L^{-1}$;	254.04	6
CTC	Ag_3PO_4/MIL-53(Fe)	pH=7.00; T=25 °C; adsorbent: 0.50 $g \cdot L^{-1}$;	12.00	7
CTC	APT/C@NiFe-LDHs	pH=4.23; T=25 °C; adsorbent: 1.00 $g \cdot L^{-1}$;	308.21	8
CTC	Calcium-rich biochar	pH=6.00; T=25 °C; adsorbent: 1.00 $g \cdot L^{-1}$;	1432.30	9
CTC	Wheat straw	pH=3.00-4.00; T=25 °C; adsorbent: 0.50 $g \cdot L^{-1}$;	23.76	10
CTC	**JLUE-MOG-3**	**pH=6.00; T=25 °C; adsorbent: 1.00 $g \cdot L^{-1}$;**	**1841.62**	**This work**
CTC	**JLUE-MOG-4**	**pH=6.00; T=25 °C; adsorbent: 1.00 $g \cdot L^{-1}$;**	**1600.00**	**This work**
CTC	**JLUE-MOG-5**	**pH=6.00; T=25 °C; adsorbent: 1.00 $g \cdot L^{-1}$;**	**1396.65**	**This work**

Table S6 Values of thermodynamic parameters for the CTC adsorption by JLUE-MOG aerogels.

JLUE-MOGs	T (K)	K_L (L·mol^{-1})	ΔG (kJ·mol^{-1})	ΔH (kJ·mol^{-1})	ΔS (J·K^{-1}mol^{-1})
JLUE-MOG-3	288	7060.16	-21.22	21.80	149.30
	298	9368.88	-22.66		
	308	12569.14	-24.17		
JLUE-MOG-4	288	7158.07	-21.25	28.35	172.37
	298	11203.49	-23.10		
	308	15156.15	-24.65		
JLUE-MOG-5	288	2865.29	-19.06	40.25	205.74
	298	4684.44	-20.94		
	308	8312.43	-23.11		

Table S7 ANOVA for the optimized response surface quadratic model.

Source	**Sum of Squares**	**df**	**Mean Square**	**F Value**	**P-value Prob > F**	
Model	595.89	14	42.56	9.72	< 0.0001	**Significant**
A-Temperature	107.21	1	107.21	24.48	0.0002	
B-Adsorbent concentration	172.05	1	172.05	39.28	< 0.0001	
C-Initial pH	1.43	1	1.42	0.33	0.5765	
D-Initial CTC concentration	34.75	1	34.75	7.93	0.0130	
AB	78.15	1	78.15	17.84	0.0007	
AC	27.88	1	27.88	6.36	0.0234	
AD	33.70	1	33.70	7.69	0.0142	
BC	0.48	1	0.48	0.11	0.7444	
BD	50.13	1	50.134	11.44	0.0041	
CD	0.05	1	0.048	0.01	0.9177	
A^2	1.76	1	1.76	0.40	0.5353	
B^2	6.93	1	6.93	1.58	0.2278	
C^2	1.60	1	1.60	0.36	0.5550	
D^2	1.29	1	1.29	0.29	0.5956	
Residual	65.71	15	4.38			
Lack of Fit	65.56	10	6.56	229.35	< 0.0001	
Pure Error	0.14	5	0.029			
Cor Total	661.60	29				
Std. Dev.	2.09		R^2		0.9007	
Mean	96.31		$R_{Adj}{}^2$		0.8080	
C.V. %	2.17		$R_{Pred}{}^2$		0.3056	
PRESS	459.41		Adeq Precision		13.379	

Supporting references

1 J. H. Miao, F. H. Wang, Y. J. Chen, Y. Z. Zhu, Y. Zhou and S. T. Zhang, *Appl. Surf. Sci.*, 2019, **475**, 549–558.

2 Y. X. Lin, S. Xu and L. Jia, *Chem. Eng. J.*, 2013, **225**, 679–685.

3 Z. Q. Li, M. Y. Qi, C. Y. Tu, W. P. Wang, J. R. Chen and A. J. Wang, *Appl. Surf. Sci.*, 2017, **425**, 765–775.

4 J. Wang, Q. F. Yao, C. M. Sheng, C. D. Jin and Q. F. Sun, *J. Nanomater.*, 2017, **2017**, 1–10.

5 W. P. Xiong, G. M. Zeng, Z. H. Yang, Y. Y. Zhou, C. Zhang, M. Cheng, Y. Liu, L. Hu, J. Wan, C. Y. Zhou, R. Xu and X. Li, *Sci. Total Environ.*, 2018, **627**, 235–244.

6 W. P. Xiong, Z. T. Zeng, X. Li, G. M. Zeng, R. Xiao, Z. H. Yang, Y. Y. Zhou, C. Zhang, M. Cheng, L. Hu, C. Y. Zhou, L. Qin, R. Xu and Y. R. Zhang, *Chemosphere*, 2018, **210**, 1061–1069.

7 L. C. Xie, Z. H. Yang, W. P. Xiong, Y. Y. Zhou, J. Cao, Y. R. Peng, X. Li, C. Y. Zhou, R. Xu and Y. R. Zhang, *Appl. Surf. Sci.*, 2019, **465**, 103–115.

8 J. Tang, B. Mu, L. Zong and A. Q. Wang, *J. Clean. Prod.*, 2018, **172**, 673–685.

9 Q. Xu, Q. Zhou, M. M. Pan and L. C. Dai, *Chem. Eng. J.*, 2019, DOI: https://doi.org/10.1016/j.cej.2019.122705.

10 Y. Y. Shao, Y. Gao, Q. Y. Yue, W. J. Kong, B. Y. Gao, W. G. Wang and W. Q. Jiang, *Chem. Eng. J.*, 2020, **379**, 122384–122392.